



# Rapid prototyping of a modular optical flow cell for image-based droplet size measurements in emulsification processes

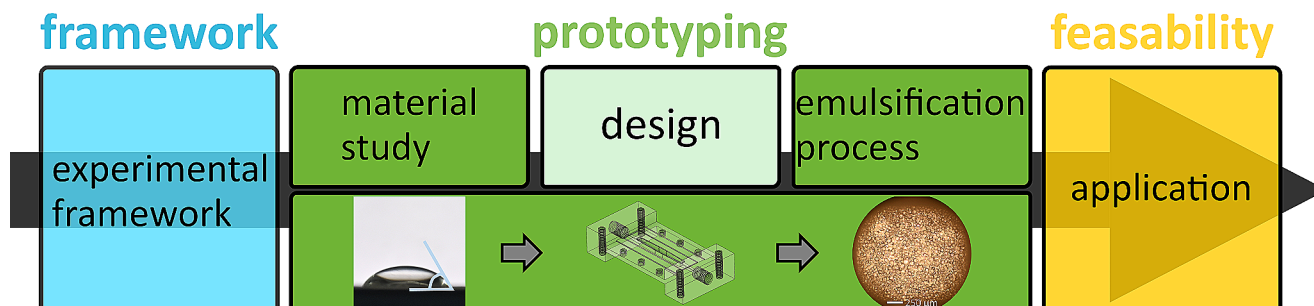
Inga Burke<sup>1</sup> · Christina Assies<sup>1</sup> · Norbert Kockmann<sup>1</sup>

Received: 11 January 2024 / Accepted: 5 March 2024  
© The Author(s) 2024

## Abstract

Emulsification processes are often found in the process industry and their evaluation is crucial for product quality and safety. Numerous methods exist to analyze critical quality attributes (CQA) such as the droplet sizes and droplet size distribution (DSD) of an emulsification process. During the emulsification process, the optical process accessibility may be limited due to high disperse phase content of liquid-liquid systems. To overcome this challenge, a modular, optical measurement flow cell is presented to widen the application window of optical methods in emulsification processes. In this contribution, the channel geometry is subject of optimization to modify the flow characteristics and produce high optical quality. In terms of rapid prototyping, an iterative optimization procedure via SLA-3D printing was used to increase operability. The results demonstrated that the flow cell resulting from the optimization procedure provides a broad observation window for droplet detection.

## Graphical abstract



## Article highlights

- 3D printed optical flow cell for optical process monitoring of an emulsification process.
- Image-based evaluation of the optical access to the emulsion by prototypes.
- Iterative approach with liquid-liquid test substance systems in flow.
- Wide operating window for successful optical measurement.

**Keywords** Emulsification process · Rapid prototyping · Optical access · Process monitoring · Image evaluation

✉ Inga Burke  
inga.burke@tu-dortmund.de

✉ Norbert Kockmann  
norbert.kockmann@tu-dortmund.de

<sup>1</sup> Department of Chemical and Biochemical Engineering,  
Laboratory of Equipment Design, TU Dortmund University,  
Emil-Figge-Str. 68, 44227 Dortmund, Germany

## Introduction

Emulsification processes and their evaluation are crucial for efficiency and quality measures of a variety of products, including food, cosmetics, and pharmaceutical preparations [1, 2]. A critical characteristic of emulsions is the droplet size distribution (DSD), which plays a central role in determining the quality of the product as well as the emulsification process performance. Evaluation and analysis of the DSD are often performed offline, which can result in inefficient process control based on the delay through the offline analysis [3, 4]. Nevertheless, automated online methods for image evaluation are increasingly used in the process industry, whose potential can be used to determine characteristic emulsion parameters, too [5–10]. The application of these image-processing methods requires optical accessibility of the emulsion. Previous investigations [5] show limitations in the optical accessibility regarding higher disperse phase fractions. Improving optical accessibility can overcome limitations caused by high oil content in emulsions for single droplet detection.

Previous investigations of the Laboratory of Equipment Design at TU Dortmund University focused on liquid-liquid microfluidic applications, multiphase flow, evaluation of different sensors for measurement in continuous capillary flow, and small-scale application [11–16]. Based on this, the current contribution describes a modular, optical measurement flow cell for improved optical access to an emulsification process and its design workflow. A qualitative evaluation of the resulting emulsion images for image processing is carried out. The concept for the development of optical measurement cells takes three key factors during prototyping into account regarding the measurement cell design: device material, channel geometry, and suitability for emulsions, which are all considered in the prototype development.

Rapid prototyping of different optical flow cells was realized using SLA-3D printing, which provides flexible design structures and results in an optimized optical measurement flow cell. 3D printing enables the production of complex and precise microfluidic structures that would be difficult to implement using conventional manufacturing methods. This

is especially important because many microfluidic systems are based on precise channel geometries and structures. The challenges of 3D printing presently relate to the choice of appropriate materials and printing resolution, which affects the limitation of the smallest channel dimensions that can be manufactured [17, 18]. The evaluation of the different prototypes of the optical measurement flow cell was carried out using different evaluation criteria based on the flow, material choice, and flow cell geometry as well as the analysis of the resulting emulsion images taken during the emulsification process. Here, it is necessary to ensure that the objects have sufficient contrast with the background and that the edges are clear and sharp [3, 19, 20]. Figure 1 illustrates the general procedure of the flow cell development, which is presented and evaluated in this contribution.

## Framework

The experimental setup as well as the used substance systems build the framework for the measurement flow cell design. Based on this the geometry as well as the material are chosen. The substance system determines the characteristics of the emulsion and thus influences the flow behavior of the product. The experimental framework and the manufacturing technology used for the modular measurement cell are presented below. The substance system used for testing and the lab emulsification process is presented. Commercially available sunflower oil ( $\nu = 65.22 \cdot 10^{-6} \text{ m}^2 \cdot \text{s}^{-1}$  at  $T = 20 \text{ }^\circ\text{C}$ ) was dispersed in deionized water ( $\nu = 1.005 \cdot 10^{-6} \text{ m}^2 \cdot \text{s}^{-1}$  at  $T = 20 \text{ }^\circ\text{C}$ ) for all experimental trials [21, 22]. The emulsion itself is produced by the high shear rates in the gap between the rotor and stator.

## Experimental Framework

The newly developed optical measurement flow cell is integrated into a laboratory emulsification process first. A schematic representation of this is shown in Fig. 2a). The emulsion process takes place in a 1 L double-jacketed glass vessel, which is temperature-controlled by a Pilot ONE

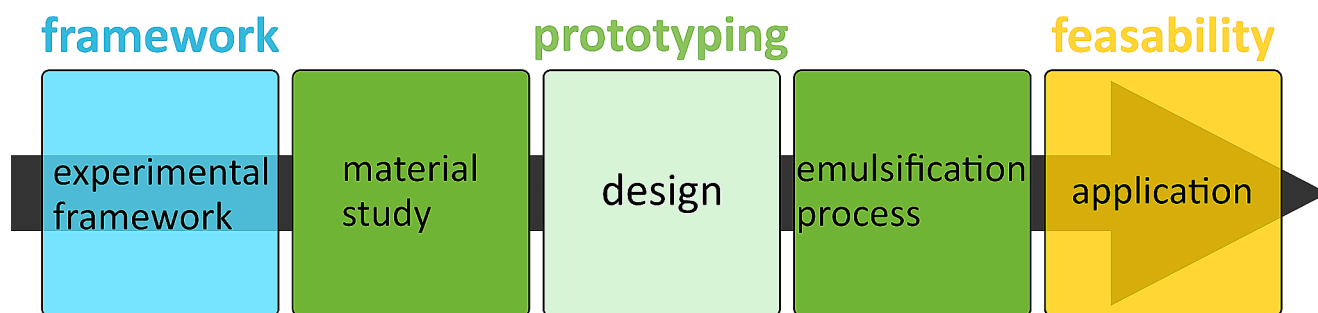


**Fig. 1** General procedure to develop a modular, optical measurement flow cell for emulsification processes

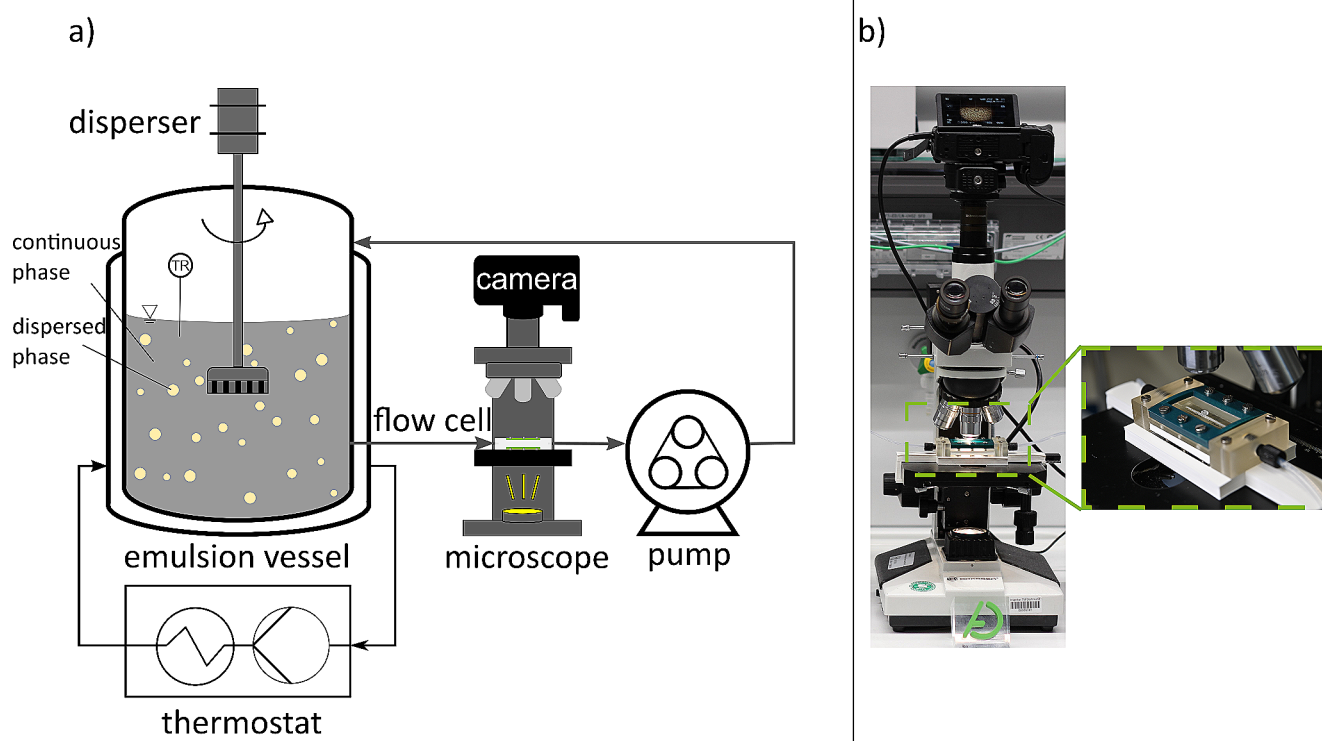


**Fig. 2** (a) Schematic experimental setup of the emulsification process including bypass with the optical measurement flow cell. (b) Detailed view of the optical measurement flow cell placed under the microscope for optical accessibility of the emulsion

ministat 230 (Huber Kältemaschinenbau AG, Offenburg, Germany). A rotor-stator system is used for emulsion production. The disperser used (HG-15D, witeg Labortechnik GmbH, Wertheim, Germany) is equipped with a dispersing tool (HT1018, witeg Labortechnik GmbH) whose rotor has a diameter of 20 mm and stator of 25 mm, resulting in a gap width of 0.25 mm. At the bottom and top, the vessel contains screw connections to which a bypass is connected.

The optical measurement flow cell is used to monitor the emulsification process and determine the emulsion quality. The bypass consists of an FEP tube with an inner diameter of 1.6 mm. Figure 2b) shows a more detailed representation of the optical analysis unit, composed of the measurement flow cell placed under a microscope (Bresser Science ADL 601P, Bresser GmbH, Rhede, Germany), with a camera (Z6, Nikon GmbH, Japan) attached. A peristaltic pump (Watson Marlow, Rommerskirchen, Germany) pumps the emulsion through the bypass, passing the flow cell and microscope before returning to the emulsion vessel. To avoid limitations due to a high droplet density during measurement in the vessel, the measurement is carried out in a bypass.

Droplet size measurement using image analysis is time-consuming because it requires the processing of a large number of droplets to build the droplet size distribution. Artificial Intelligence (AI) algorithms offer high effectiveness in the field of image recognition, thus the image quality

**Table 1** Camera settings for experimental trials

Camera setting	Specification
Shutter speed / s	1/500 & 1/1,000
ISO / -	800 & 1,000
Frames per seconds / s <sup>-1</sup>	30
Quality / p	3,840 × 2,160
Color temperature / K	2,800

of the resulting images is evaluated for the possibility of AI-based evaluation [23]. The pixel-to-micrometer ratio is essential to determine the specific droplet size of the disperse phase. For this purpose, a scaling frame was designed, which is centered in the field of view on the modular, optical measurement flow cell with internal dimensions of 1.5 mm x 2 mm. An image capture including the 3D printed scaling frame to identify the pixel-to-micrometer ratio illustrated in Fig. S1 in Supporting Information. The general camera settings during the experimental execution are listed in Table 1. The images were captured at a resolution of 2160 p, resulting in a pixel-to-micrometer ratio of 1.27 p·μm<sup>-1</sup> using the scaling frame.

Table 2 defines the operating window examined for the characterization of the presented optical measurement flow cell.

**Table 2** Process parameter settings and conditions as well as the used operation range

Process parameter	Operation range
Continuous phase / vol.-%	99 – 85
Disperse phase / vol.-%	1–15
Total volume / mL	1,000
Disperser speed $U$ / rpm	5,000 & 10,000
Temperature $T$ / °C	25.00
Volumetric flow rate bypass $\dot{V}_{\text{side stream}}$ / mL·min <sup>-1</sup>	42.39

**Table 3** Requirements and evaluation criteria for the optical measurement flow cell and their importance during prototyping; + very important, o important, - less important

Specification	Requirements	Importance
Flexibility	Variation of phase fraction, microscopic magnification	o
Geometry	Channel depth for light penetration	+
Flow	No dead zones, no back flow, no vortex formation, flow velocity, and shutter time	o
Material	Wettability, lipophilic, stability, tightness, resistant to detergents	+
Optical	Low optical distortion, transparent, light transmittance	+
Other	Fixations and attachment, fast procurement of spare parts, cheap	-

## Manufacturing for Prototyping of Optical Flow Cell

The measurement flow cell components, from which the various prototypes are made, are manufactured using additive fabrication, in this case, stereolithography (SLA). In SLA printing, the components are manufactured with a high resolution of 0.025 – 0.100 mm by photo-induced polymerization using an SLA-3D printer (Formlabs Form 3+, Formlabs, Berlin, Germany). Various resins with different properties are used for this purpose. A list of the used resins is given in Table S1 in Supporting Information.

The surface of the printing platform is immersed in a liquid resin solution and polymerized layer by layer using a (ultraviolet) UV light beam, see Fig. S2 in SI. The finished part is washed in isopropyl alcohol (IPA) for 30 min. to remove the unpolymersed liquid resin from the component. A syringe filled with IPA is used to clean internal channels and cavities to remove residues from the channels. After that, the component is UV post-cured.

## Prototyping

The flow cell was iteratively developed, which resulted in different prototypes. In general, the process covers three key factors related to the measurement flow cell design (see Fig. 1). First, the properties of different materials are investigated and a material selection is made for the presented substance system, see Sect. 3.1. The second iteration step includes the design of the optical flow cell, in particular, the channel geometry is investigated (see Sect. 3.2). The final iteration step (see Sect. 3.3) addresses the investigation of integrating the measurement cell into an emulsification process and assesses the successful droplet size determination during the process. This integration is crucial for the

final evaluation of the measurement cell for the application of an online measurement method. Iteration of the above aspects is fundamental to the development of the presented 3D printed optical flow cell.

The evaluation of the prototypes is based on multiple criteria. Here, the importance of achieving a high optical quality of the resulting emulsion images is decisive for an intended image evaluation. Single droplet detection using image processing requires high resolution and recognizability. Droplet boundaries need to be clear with high contrast and in focus. Sufficient exposure of samples under a microscope and the desirability of a high refractive index of the droplets are important. Capturing images in flow requires minimal motion blur. A high number of recorded images per second is crucial as well as an adaptation of the shutter speed to the flow velocity. Capturing videos provides continuous monitoring of process changes and recording of a statistically significant number of droplets [24, 25]. A transparent material with low optical distortion is required for the measurement flow cell to be able to detect single droplets across the operating window. Preventing coalescence of the droplets in the bypass (see Sect. 2.1) and the optical flow cell are relevant, too. The material properties of the flow cell are important to avoid coalescence especially if no surfactants are used. The flow through the measurement cell is crucial. Back-mixing, the formation of vortices, and flow detachment must be avoided so that coalescence is prevented on the one hand and droplet formation on the other hand. An overview of all defined requirements, evaluation criteria, and their importance for the optical measurement flow cell design are given in Table 3.



## Material Study

The iterative workflow of this design step, illustrated in Fig. 3, focuses on determining all requirements concerning the components. Further, a wetting test on all needed components is necessary. Finally, the resulting contact angles are evaluated for the subsequent application.

The investigation of the wetting behavior of the materials used is crucial in the development and design of an optical measurement flow cell. The materials have to be selected in a way that especially the disperse phase does not adhere to the flow channel material and coalesces there. Thus, when investigating water and oil droplets, high contact angles  $\Theta > \sim 90^\circ$  are desirable for the respective materials.

Wettability is defined by the static contact angle  $\theta$  and depends on the properties of the solid surface, the deposited phase, and the surrounding phase. According to the Young-Laplace equation (Eq. 1), the contact angle  $\theta$  is determined by settling a droplet of liquid on a solid surface and is defined by  $\gamma_{SG}$ ,  $\gamma_{LS}$ , and  $\gamma_{LG}$ .  $\gamma_{SG}$ ,  $\gamma_{LS}$ , and  $\gamma_{LG}$  describe the interfacial tensions between solid (S) and gas (G), liquid (L) and solid, and liquid and gas, respectively.

$$\cos\theta = \frac{\gamma_{SG} \cdot \gamma_{SL}}{\gamma_{LG}} \quad (1)$$

For contact angles  $\theta < 90^\circ$ , the deposited phase partly wets the solid surface, while for  $\theta > 90^\circ$  the deposited phase

is considered non-wetting. If  $\theta$  tends towards  $0^\circ$ , complete wetting is present and the liquid spreads across the surface [26, 27].

The material properties of the optical flow cell were examined for the wettability of water and sunflower oil using the sessile drop method. The plugin *Contact Angle* for the software *ImageJ* was used to evaluate the contact angle  $\theta$  [28].

## Wettability Test and Material Choice

The modular, optical measurement flow cell consists of different components such as a viewing glass, a measurement cell frame, seals, and an adjustable channel depth. The adjustable channel depth, the measuring cell frame, and the viewing glass are product-contacted components. Since the used materials need to confirm optical requirements as well (see Table 3), the wetting behavior of the pure substance systems is tested on High Temp resin and Clear resin for the flow cell frame and the channel depth adjustment. From the contact angles of the tested materials ( $\theta_{\text{HighTemp, Water}} = 76.0^\circ$  vs.  $\theta_{\text{Clear, Water}} = 65.5^\circ$ , and  $\theta_{\text{HighTemp, Oil}} = 38.2^\circ$  vs.  $\theta_{\text{Clear, Oil}} = 30.0^\circ$ ), it can be concluded that none has optimal properties for emulsion handling since the tested fluids -water and sunflower oil- wet all of the tested materials. Additionally, the wettability for sunflower oil and water on different materials (FEP, glass, and PMMA) used as the view glass were tested. Only FEP behaves in a dewetting manner with a

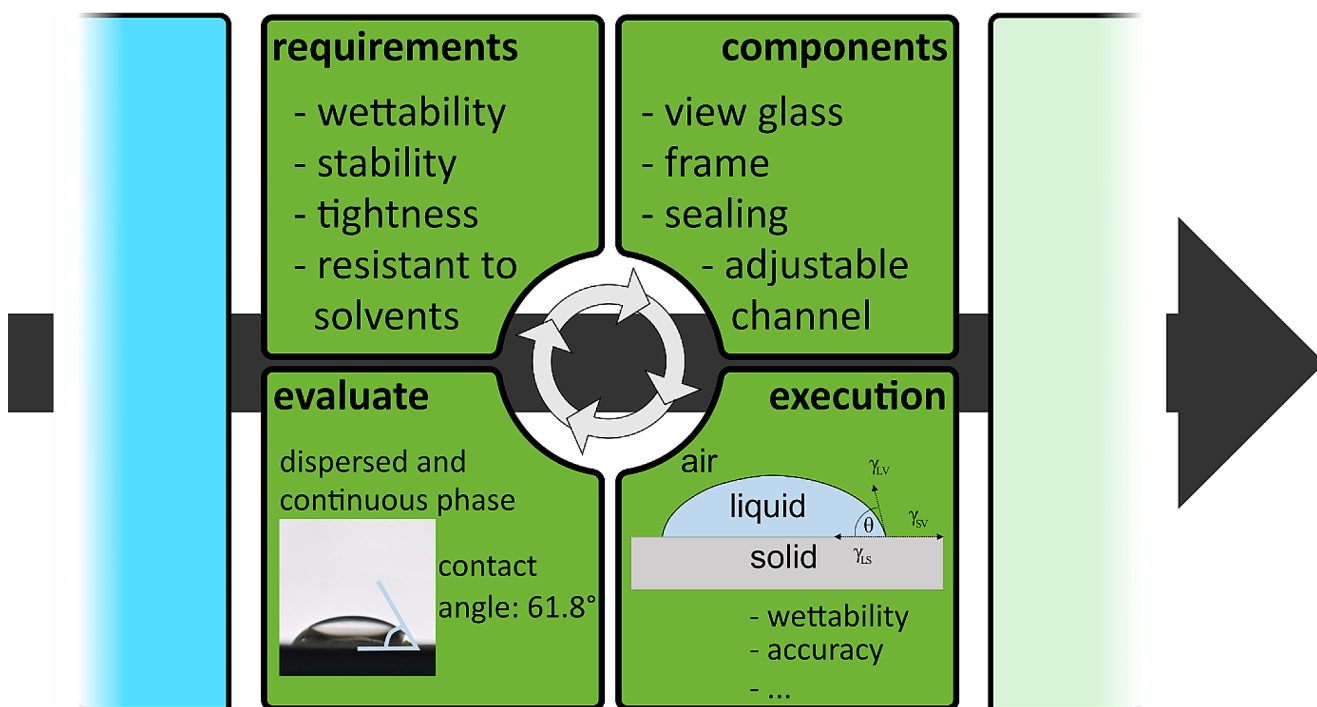


**Fig. 3** Schematic overview of the first iterative process step in prototyping for the development of an optical measurement flow cell; the iteration shows the material study including the surface conditions and wettability of the material used for the optical measurement flow cell [16]

contact angle of  $\theta = 97.0^\circ$  concerning water. For sunflower oil, a contact angle  $\theta = 83.2^\circ$  was measured. Thus, FEP repels water and sunflower oil better and has lower adhesion properties for the pure substance systems. The results of all contact angle measurements for different fluids are given in Supporting Information Sect. 3. In this application, the Clear resin is chosen, since it provides better optical properties. The wetting behavior of Clear resin implies droplet adhesion on the surfaces of the adjustable channel depth and the measurement cell frame. Coalescence is prevented by a constant flow within the optical measurement cell. If necessary a higher volumetric flow rate is adjustable. The droplets are recorded on the surface and in the center of the channel, and adhering droplets do not influence the optical evaluation. To prevent droplet adhesion at the view glass, it is covered with an FEP film. For the used substance system and process settings, coalescence within the optical measurement flow cell was not observed. Further investigations of the seals will be carried out for the final material choice.

### Design of Optical Flow Cell

The iterative workflow of the second design step, illustrated in Fig. 4, covers the channel geometry of the optical flow cell. As in the first iteration step, requirements need to be specified concerning the flow behavior. Further, a flow test of the designed measurement cell is executed and evaluated

before the design is changed to counteract the observed, unwanted effects.

The geometry of the microchannel in the flow cell plays an essential role in the characterization of optical measurement flow cells. The channel geometry needs to be designed to avoid flow detachment, vortex formation, backflow, or the development of dead zones. These phenomena are undesirable as they increase the coalescence of droplets in the optical measurement cell. The seal and its placement affect the flow behavior as well, especially if it is in contact with the emulsion, and needs to be discussed. Improper placement and inconsistent production provide potential droplet adhesion and coalescence. In addition to the channel and frame geometry, different channel depths are investigated, which have an influence on the flow, light transmission, and single droplet detection during the emulsification process. The influence of the channel depth on the image quality is discussed later.

Flow tests are carried out to characterize the optical measurement flow cells concerning their flow characteristics. The measurement cell to be investigated is attached to a stand and connected to the emulsification vessel, an upstream pump (LabDos Easy Load, HiTec Zang GmbH, Herzogenrath, Germany), and a three-way piece using an FEP tube with an inner diameter of 1.6 mm. An injection syringe filled with a defined amount of ink is connected to the three-way piece. The flow test is recorded using a

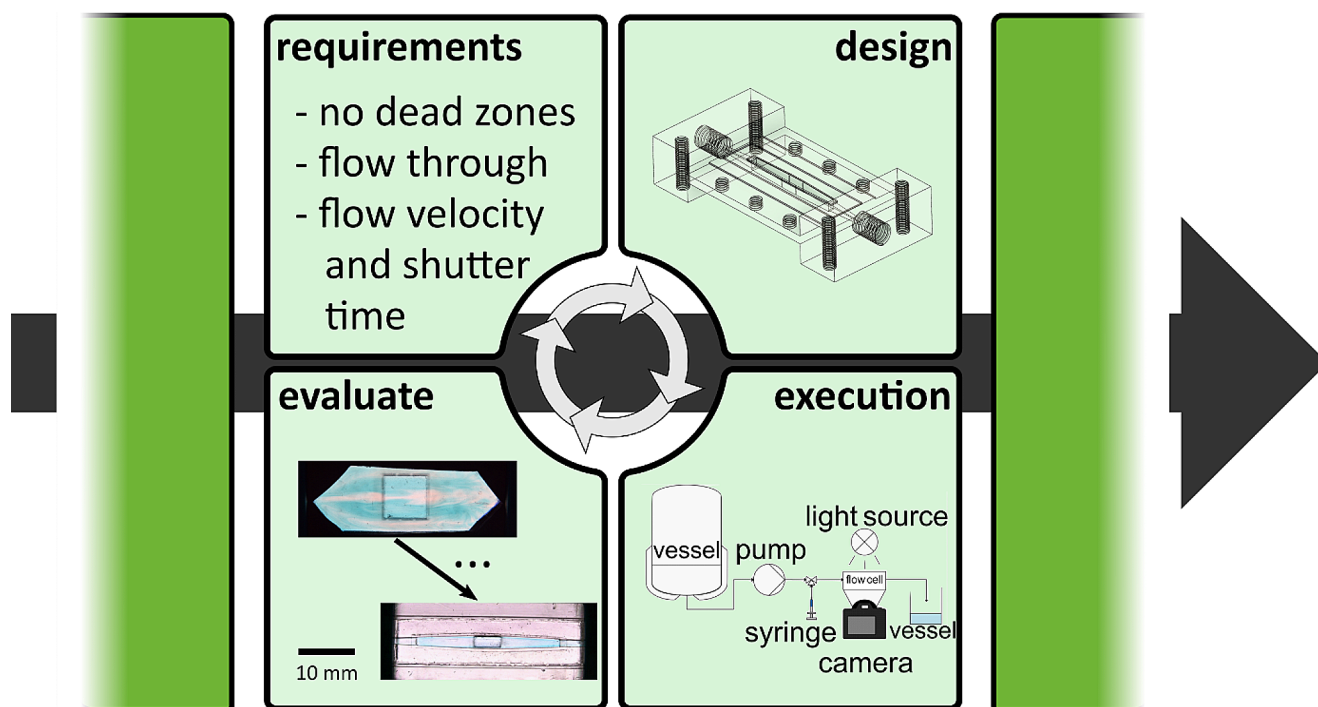


**Fig. 4** Schematic overview of the second iterative process step in prototyping for the development of an optical measurement flow cell; the iteration shows the steps and requirements concerning the channel

geometry and flow characteristics of the flow cell including the examination of different seals [16]

Nikon Z6 system camera. The pump was set for different volumetric flow rates and initially pumped deionized water through the optical flow cell. For flow observation, ink from the syringe was added in short pulses to the process. Knowledge of the flow regime is essential in flow monitoring. This is determined for the respective volumetric flow rates using the dimensionless Reynolds number  $Re$ . The Reynolds number is given by

$$Re = \frac{u \cdot \rho \cdot d_h}{\eta} = \frac{u \cdot d_h}{\mu}, \quad (2)$$

and is defined as a function of mean velocity  $u$ , density  $\rho$  of the continuous phase, hydraulic diameter  $d_h$ , dynamic viscosity  $\mu$  and kinematic viscosity  $\eta$ , where viscosity depends on temperature. The hydraulic diameter  $d_h$  depends on the cross-section of the channel and is defined for the smallest cross-section in the measurement cell, i.e. the observation window, by

$$d_h = \frac{4 \cdot A}{P}, \quad (3)$$

where  $A$  is the cross-sectional area and  $P$  the perimeter. For a straight tube, laminar flow exists for  $Re < 2300$ , and turbulent flow exists for  $Re > 2300$ . The velocity  $u$

$$u = \frac{\dot{V}}{A}, \quad (4)$$

corresponds to the quotient of volumetric flow rate  $\dot{V}$  and the cross-sectional area  $A$  [29].

### Channel Geometry and Design

In the following, the flow test results of the additive-manufactured prototypes are presented and discussed. Besides the channel geometry, the influence of different seal materials and seal manufacturing is carried out. The channel width is changed from 15.00 mm to 2.50 mm for Prototype 1 to 6. Besides the channel geometry, the seal and the design of the inlet into the flow cell were changed during prototyping.

Figure 5 A) shows an overview of the particular flow phenomena of the different prototypes with varying micro-channel shapes and the influence of different seal materials and manufacturing and their effect on the flow.

Figure 5 A) Prototype 1 shows backmixing and vortex formation, which needs to be prevented. Both phenomena influence the droplets of an emulsion in the measurement cell, probably resulting in changes in droplet shape and size. The channel in Prototype 2 is therefore narrowed, but the phenomena still occur. In Prototype 3, the channel inlet into the optical observation window was changed and instead of backmixing and vortex formation, flow detachment took place. Since the flow detachment happens at the channel enlargement, the channel in Prototype 4 and Prototype 5 was designed much narrower (8.00 mm to 2.50 and 3.00 mm). The flow characteristics of the two prototypes hardly differ. Prototype 5 was preferred for further investigation, because of the 0.5 mm wider channel geometry.

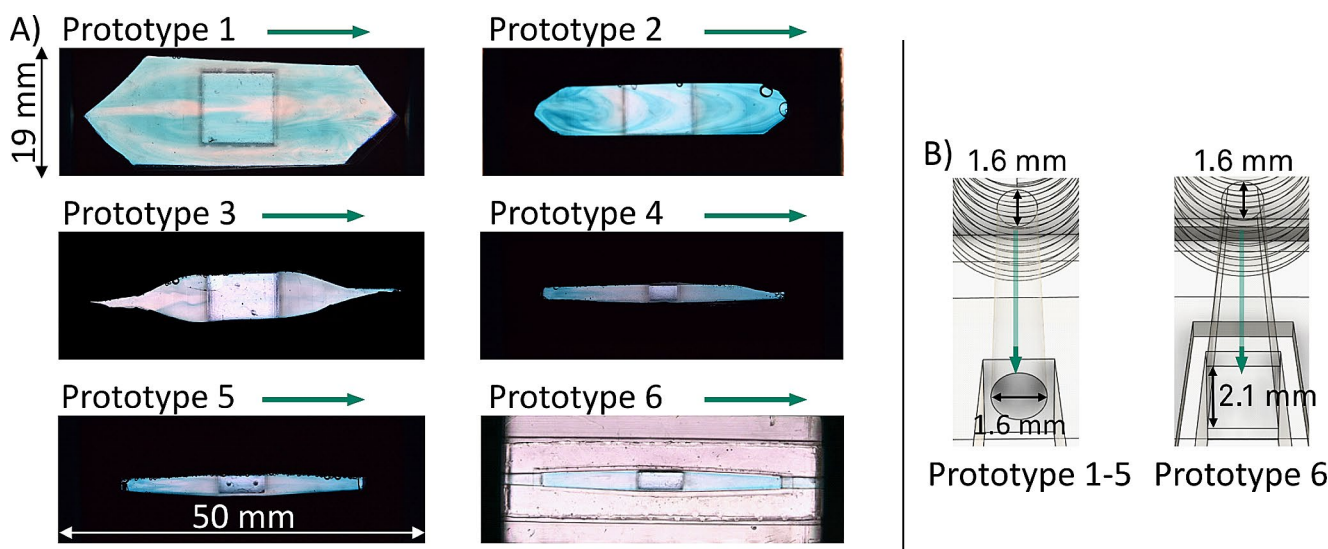


**Fig. 5** (A) Images of flow test trials of the different Prototypes (1–6) showing the observation window. The flow direction is given by the arrow and is from left to right. The channel geometry was changed during prototyping with a special focus on the channel width and the flow behavior in the optical measurement flow cell for a mean flow

velocity of  $35.8 \cdot 10^{-6} \text{ m} \cdot \text{s}^{-1}$  at the inlet of the flow cell. During prototyping the material of the used seal was examined. The seal used in Prototype 1–5 is a silicone mat and in Prototype 6 a 3D printed seal is used. (B) Variation of the channel inlet including flow direction as a result of the prototyping during the execution of flow tests

A wider channel geometry results in lower flow velocities at the same volumetric flow rates, less impact on the droplets as well as in capturing droplets without motion blur. Both Prototypes (4 and 5) still show slight boundary layer separation, resulting in vortex-like dead zones at the inlet. Compared to Prototype 6, where the seal material and thus the manufacturing was changed, this slight boundary layer was further reduced. The uneven silicone seal geometry and the contact between the seal and the medium can influence the flow behavior. Despite its unfavorable wetting behavior, the seal for Prototype 6 was 3D printed and embedded in the flow cell frame. In this way, there is significantly less contact between the flow and the seal and thus the wetting behavior of the material has less influence. Further, the channel inlet was adapted to the channel geometry (from straight to angled), showing a positive effect on avoiding boundary layer separation. For illustration, the different channel inlets (LHS: inlet Prototype 1–5, RHS: inlet Prototype 6) are shown in Fig. 5B).

The cross-section of the modular optical measurement flow cell is adjustable between 0.25 and 1.5 mm and is achieved in the middle of the flow cell. There, the observation of the emulsion in the process is carried out.

### Emulsification Process

The next step of the iterative workflow, illustrated in Fig. 6, focuses on the implementation and the functional test of

the designed prototype for emulsification processes. Here the requirements are evaluated using the resulting emulsion images and are evaluated using an AI-based image detection method.

The suitability of the modular optical measurement flow cell for emulsification processes is crucial for its final application. The additively manufactured flow cell is based on a modular principle to enable flexible variation of the channel depth. When using a low channel depth, the transmission of light intensity through the emulsion is advantageous. The same flow rate for smaller cross-sections means higher flow velocity resulting in some disadvantages. On the one hand, a higher flow velocity implies an increased pressure drop as well as a shorter residence time within the optical measurement flow cell. A higher velocity in the optical measurement flow cell minimizes the risk of coalescence; on the other hand, for faster droplets, a shorter exposure time or a high number of frames per second is required to capture sharp droplet images. Additionally, sufficient exposure is necessary. Thus, the flow velocity is linked to a technical limit regarding the exposure of emulsion images without motion blur.

Dispersion experiments are performed to study the influence of different channel depths concerning image evaluation as well as the resulting droplet size and droplet size distribution. Individual video sequences were recorded for single droplet detection and droplet size determination to evaluate the process progress using the optical measurement

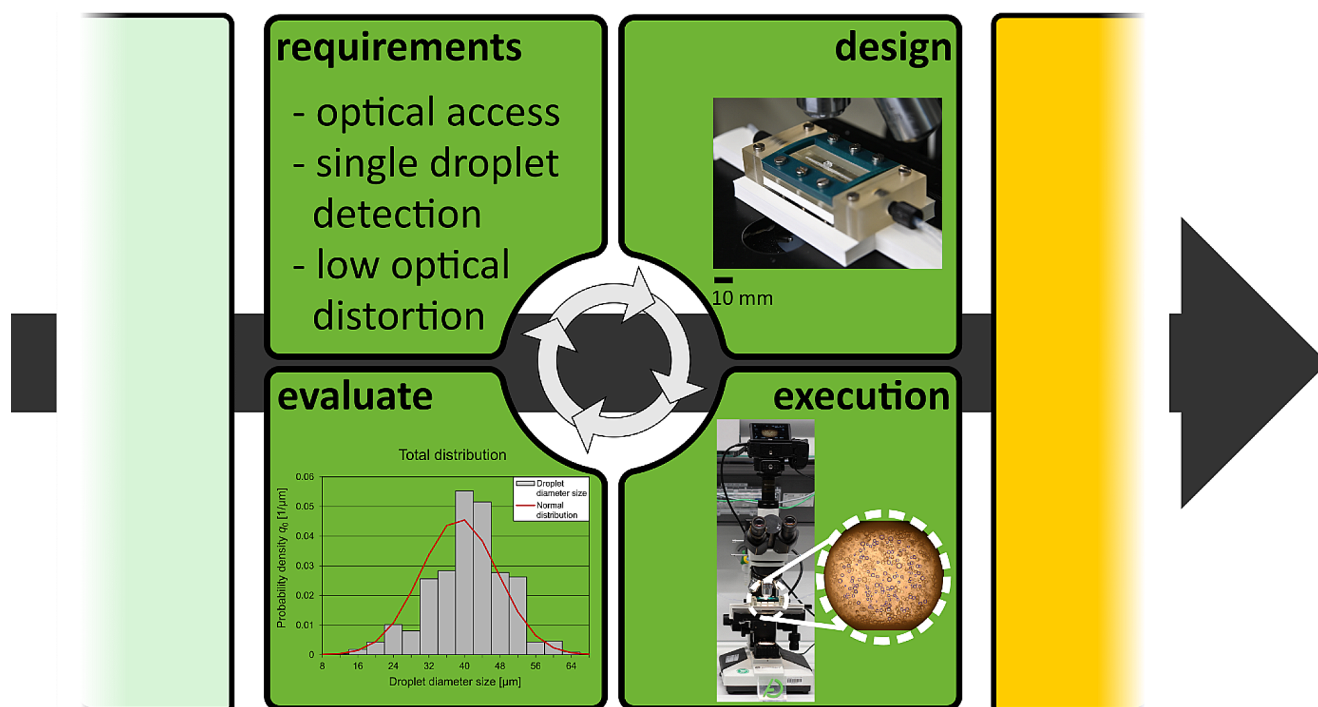


**Fig. 6** Schematic overview of the third iterative process step in prototyping for the development of an optical measurement flow cell; the iteration shows the implementation and optical parameters of the flow cell, lighting, and digital camera (entire system) during an emulsification process [16]



flow cell for optical access. The total list of process parameters is listed in Table 2.

### Suitability of Optical Flow Cell for Emulsification Process

As shown in Fig. 7, the dependence of the phase fraction of the disperse phase on the image quality and the clarity of the droplet edges is evident at constant channel depth. The phase fraction also influences the light transmission of the emulsion. An increasing number of droplets, which occurs with a higher amount of disperse phase, leads to a stronger deflection of the light and thus to an attenuation. A decrease in the lighting can be noticed for the same camera settings in a) to c). An adjustment of the exposure time as well as the ISO value, as already done for Fig. 7d), is feasible to counteract this effect. However, adjusting the ISO value and the shutter speed shows less clear droplet edges, also due to the increase in the volumetric phase fraction. A “sweet spot” needs to be found to avoid motion blur and image noise affecting the image quality.

### Final Prototype - Optical Flow Cell

The final prototype of the total iterative process for developing the optimal design of an optical measurement flow cell, presented in Fig. S6, results in a modular design. An explosion view of the modular, optical measurement flow cell is shown in Fig. 8a).

The entire optical flow cell consists of a 3D printed flow cell frame, seals on top and bottom of the frame, an adjustable channel depth, a FEP-covered (FEP film, SOOWAY) view glass, and a PLA frame at the top and bottom. The 3D printed PLA frames provide mechanical strength and are used to connect the individual components. The measurement flow cell frame defines the channel geometry of the optical flow cell as described in Sect. 3.2 and the fluidic connections (UNF 1/4–28 flat bottom) to the side stream. The frame is made of Clear resin to provide optical access. Although the material does not show non-wetting behavior regarding the disperse phase, the material is used here. The first test regarding the coalescing of droplets, as can be

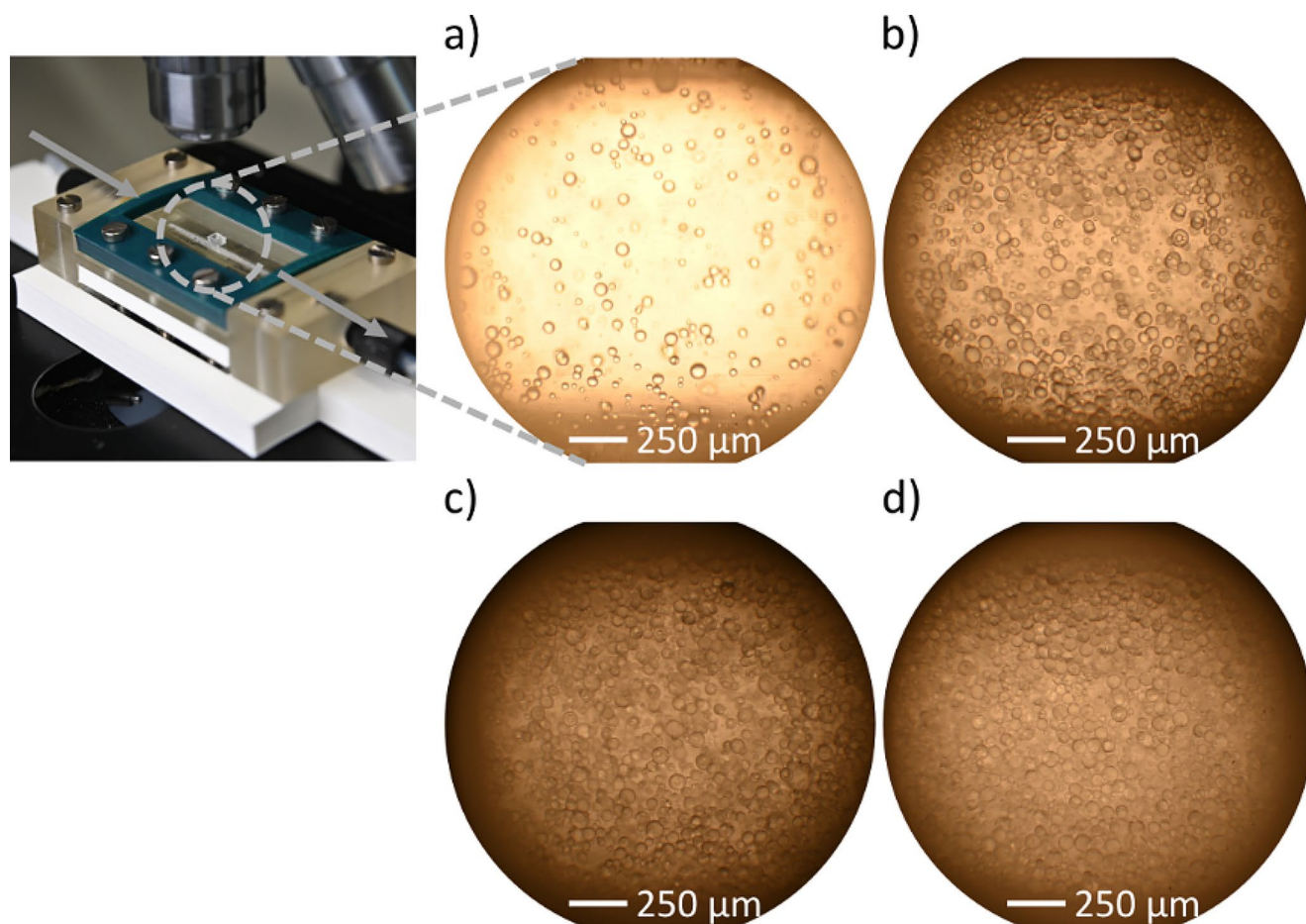


**Fig. 7** Microscopic images of emulsions with different content of disperse phase captured in the optical measurement flow cell with a channel depth of 0.25 mm for (a) 1 vol.-%, (b) 5 vol.-%, (c) 10 vol.-%, and (d) 15 vol.-%. a)- d) showing the same point in time for the same

process parameters ( $t_{\text{process}} = 35$  min,  $U_{\text{dispenser}} = 5000$  rpm) and light source. Camera settings for a)- c): ISO 1000 and shutter speed 1/1000 s and for d) ISO 1000 and shutter speed 1/500 s



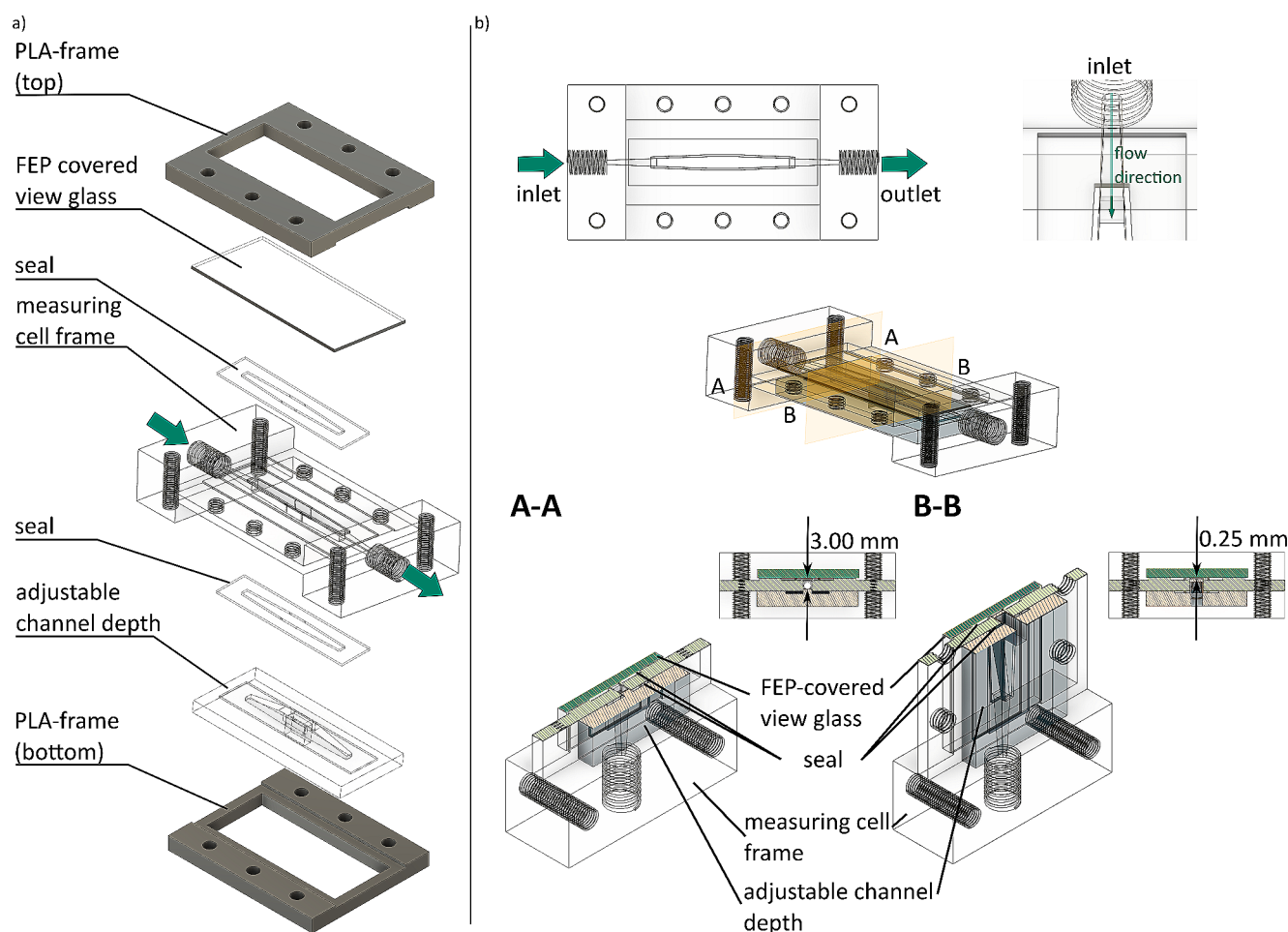


**Fig. 8** (a) Explosion view of the modular optical measurement flow cell. (b) Top view of the optical flow cell as well as a closer view of the channel inlet. A-A and B-B show two sectional views of the optical flow cell directly after the inlet and in the middle at the observation window

seen in Sect. 4, shows that the material selection does not affect the optical accessibility, and adhesion or coalescence of the droplets is not observed. The modular design is used to change only the dimensions of the channel depth adjustment (Clear resin) to cover flexible, adapted dimensions of the flow-through within the observation window. Varying the dimension of the adjustable channel depth provides a change in the cross-section B-B as can be seen in Fig. 8b). The final channel depth of 0.25 mm shows promising results for the given use case. The channel depth adjustment is made of Clear resin, as the material must be translucent for the transmitted light method used here for droplet detection. Using an FEP-covered (0.15 mm thick) view glass (2 mm thick PMMA) for optical access forms the upper part of the optical measurement flow cell. Both, the FEP-covered view glass and the adjustable channel depth, are connected to the measurement cell frame using a 3D printed PLA frame at the top and bottom. To prevent leakage two 3D printed seals (Elastic 50A resin) are used. The final geometry of the optical flow cell is shown in Fig. 8b), too. The channel width

is 3 mm at the observation window and the inlet features a cross-sectional change from a circular to a rectangular cross-section.

## Feasibility Study

The optical measurement flow cell is applied for the optical evaluation of an emulsification process. The flow cell is evaluated based on the criteria established in Sect. 2.3 and is executed qualitatively concerning a potential single droplet evaluation based on the resulting images. First, the influence of the energy input and consequently of the resulting droplet size is investigated for a sunflower oil content of 10 vol.-%. The channel depth of the optical measurement flow cell is the minimum adjustable depth of 0.25 mm. The process conditions, as well as the camera settings, are kept constant. Figure 9 shows example images captured in the optical measurement flow cell.

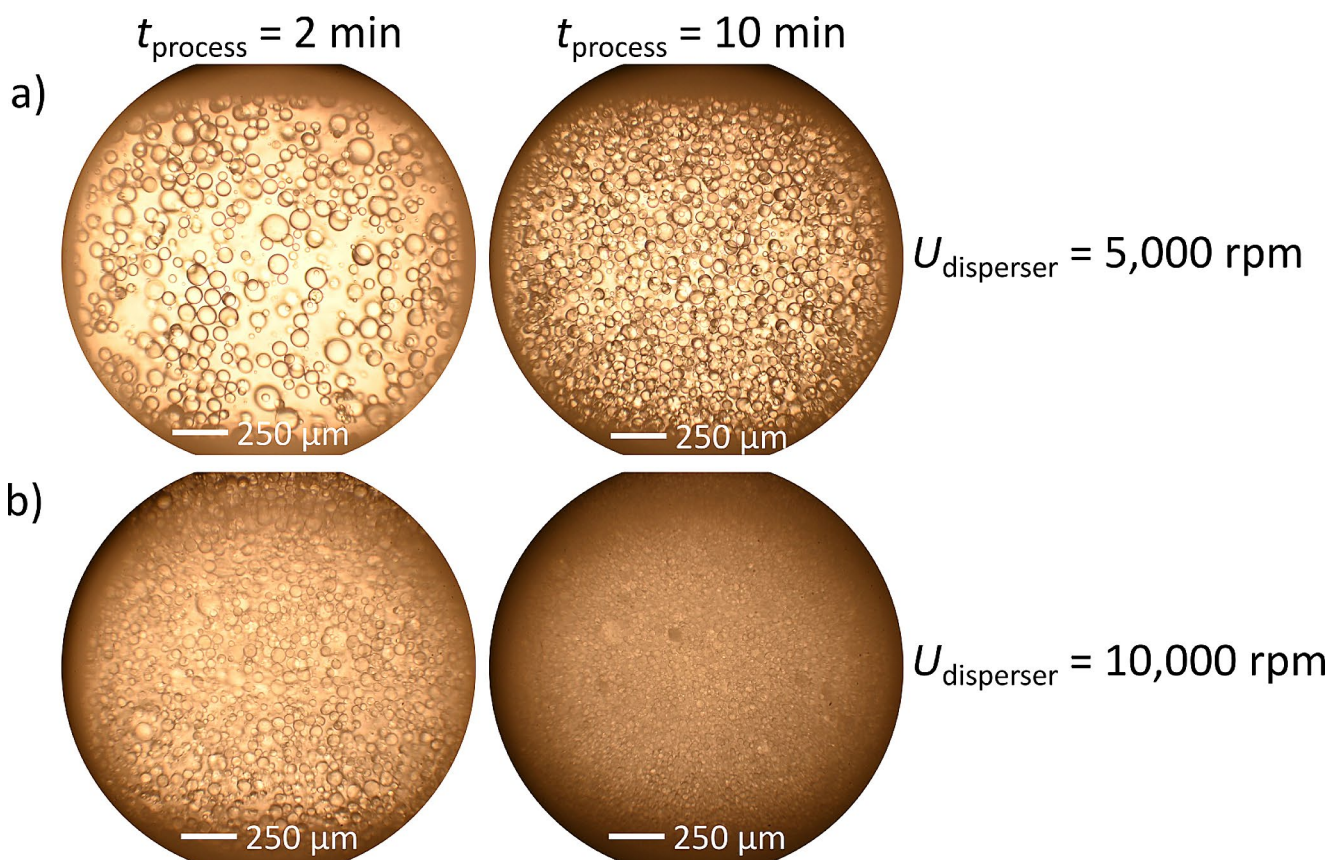


**Fig. 9** Microscopic images of emulsions captured in the optical measurement flow cell with a channel depth of 0.25 mm for the same phase fraction of the disperse phase (10 vol.-%) and different disperser speeds. Images on the LHS, after  $t_{\text{process}} = 2$  min and images on the

RHS after  $t_{\text{process}} = 10$  min; **(a)**  $U_{\text{dispenser}} = 5000$  rpm, **(b)**  $U_{\text{dispenser}} = 10,000$  rpm. Camera settings for a): ISO 1000 and shutter speed 1/1000 s and for b) ISO 1000 and shutter speed 1/400 s

Comparing the same points in time for the different disperser speeds, it is noticeable that the droplet edges are visualized less clearly at higher energy input. While the edge detection of the droplets for the lower energy input (see Fig. 9a) is clear for both process times. This is not the case in b). The contrast between the continuous phase and the disperse phase decreases with an increase in the number of droplets. With the same volumetric phase fraction of sunflower oil, but a higher energy input, more, smaller droplets are dispersed in the continuous phase. The refraction caused by the increase in the number of droplets leads to a reduction in the optical contrast between the two phases. For  $U_{\text{dispenser}} = 5000$  rpm, the contrast between the continuous phase and the disperse phase is high enough to recognize the edges of the individual droplets well. Using an AI-based droplet detection method [5] with a confidence score of 0.6, in (a) 259 (LHS) and 538 (RHS) droplets are detected. The higher energy input shown in b) leads to more and smaller droplets, which reduces the optical contrast and thus the edge detection. Overlapping of the individual droplets reduces the light transmission of the emulsion. The number of detected droplets in b) decreases to 155 and 68 detected

droplets, respectively. The corresponding DSDs are shown in Fig. S9 in Supporting Information.

The optical measurement cell is used to analyze the droplet sizes of different emulsions. Investigating the influence of different channel depths at constant process conditions, as shown in Fig. 10, a lower channel depth shows an increase in brightness and contrast.

The reduced channel depth leads to better light transmission through the emulsion and thus a better edge imaging of the droplets. As shown in the corresponding histograms of the droplet size distributions, in Fig. 10b) a smaller number of droplets (112 to 491) are detected via the AI-based droplet detection. For both detections, the same configurations and in particular the same confidence score of 0.6 were applied. This confidence score allows the detection of a large number of smaller droplets but also increases the detection of larger droplets. Although the number of droplets detected decreases with increasing channel depth (a) to b)), both histograms show a normal distribution. However, the class width and number decrease due to the reduced number of detected droplets in b), resulting in a distribution

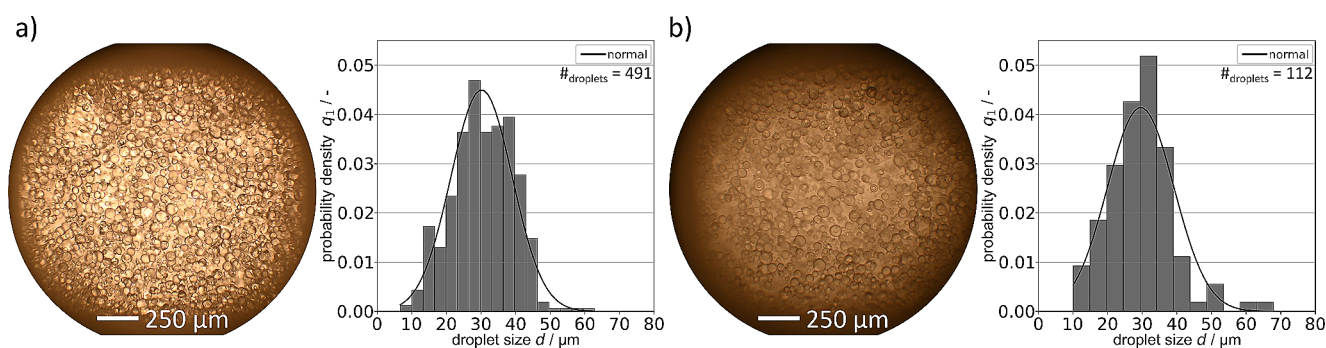


**Fig. 10** Microscopic images of emulsions with the same phase fraction of the disperse phase (10 vol.-%) captured in the optical measurement flow cell with different channel depths, (a) 0.25 mm and (b) 1.00 mm, and the corresponding histogram of droplet size distribution. Both

images show an emulsion proceeds with the same process and camera settings ( $U_{\text{dispenser}} = 5000$  rpm after  $t_{\text{process}} = 35$  min). The confidence score is set to 0.6 for AI-based droplet detection

with less statistical relevance and potentially not reflecting the droplet size distribution of the emulsion.

A drawback of a reduced channel depth is the flow velocity. For the same flow rate, a smaller cross-section results in higher flow velocities than a larger cross-section, making it difficult for the camera to detect droplets without motion blur. The exposure time must be adjusted for higher flow velocities. The faster the droplets pass the optical measurement flow cell, the shorter the exposure time needs to be to capture the droplets sharply and in focus. However, there is a technical limit, as better exposure is required for faster shutter speeds. The technical limit is affected by the number and size of the droplets and the channel depth of the used optical measurement flow cell. The more and smaller the droplets in the optical measurement cell become for an increasing channel depth, the more light is refracted by the droplets. As a result, it is no longer sufficient to illuminate the image with a short exposure time.

Thus, the image quality is affected by the channel depth, which leads to the conclusion that an adaptation of the channel depth to the considered substance system is necessary. A channel depth of 0.25 mm shows the most promising results for the tested application window and for the presented substance system (see SI Sect. 9).

## Conclusion and Outlook

Measuring the droplet size distribution in an emulsification process is important for its quality and efficiency. For this purpose, an optical measurement flow cell was designed and characterized based on an iterative optimization procedure including three key factors during prototyping. The material choice was performed to avoid droplet adhesion at the flow cell. The measurement cell geometry with width and depth of the observation channel and the flow characteristics within the measurement flow cell were considered,

discussed, and adapted using rapid prototyping with SLA 3D printing. This provides flexible design structures and resulted in an optimized optical measurement flow cell. At the observation window, the channel width of the optical measurement flow cell is 3 mm to have a wide inspection area. The inlet features a cross-sectional change from a circular to a rectangular cross-section for undisturbed observation. The final application of the prototypes during the last iteration step shows the suitability of the prototype for emulsion processes and concludes the successful optimization process in the measurement flow cell design. The modular design of the optical flow cell allows rapid adaptation of the observation area. Adjusting optical accessibility can widen the application window of the optical measurement flow cell related to a higher sunflower oil content or even smaller droplet sizes. In this work, the influence of different channel depths (0.25 to 1.50 mm), different volumetric phase fractions of the disperse phase as well as different disperser speeds are considered. A channel depth of 0.25 mm shows promising results for the investigated process parameters.

The optical measurement flow cell is successfully used for qualitative evaluation of emulsion images, and single droplet detection is performed after the emulsification process is finished. Using optical access to an emulsification process provides the opportunity to use object detection methods for process monitoring, evaluation, and control. The resulting images are conceivable to train and optimize an algorithm to perform droplet detection as well as droplet size measurement. By including this analysis an automated process monitoring can be performed. Additionally, further adaption to other substance systems and industrial emulsion systems is conceivable to provide a broader application window for the presented optical measurement flow cell.

## Abbreviations

AI	Artificial Intelligence
CQA	Critical Quality Attribute



DSD	Droplet Size Distribution
FEP	Fluoroethylene Propylene
G	Gas
HDT	Heat Deflection Temperature
IPA	Isopropyl Alcohol
L	Liquid
PMMA	Poly(Methyl 2-Methylpropenoate)
S	Solid
SLA	Stereolithography
UV	Ultraviolet

**Supplementary Information** The online version contains supplementary material available at <https://doi.org/10.1007/s41981-024-00323-2>.

**Acknowledgements** The authors thank Carsten Schrömges for his technical support, Stefan Höving for constructive feedback during writing process, Mr. Salzer (Ark Vision Systems GmbH & Co. KG) and Mr. Stein (SystemKosmetik Produktionsgesellschaft für kosmetische Erzeugnisse mbH) for fruitful discussions during project meetings, and the German Federal Ministry for Economic Affairs and Climate Action (BMWK) for funding this research as part of AiF (Support Code: KK5168501 PR0).

**Author contributions** The manuscript was written through the contributions of all authors. All authors have approved the final version of the manuscript.

**Funding** Open Access funding enabled and organized by Projekt DEAL. The authors thank the German Federal Ministry for Economic Affairs and Climate Action (BMWK) for funding this research as part of AiF (Support Code: KK5168501 PR0). Open Access funding enabled and organized by Projekt DEAL.

## Declarations

**Associated content** The Supporting Information (SI) is provided for this article and contains further detailed information regarding the experimental setups, materials and methods, and technical drawings of the final prototype of the measurement flow cell.

**Conflict of interest** On behalf of all authors, the corresponding authors state that there is no conflict of interest.

**Open Access** This article is licensed under a Creative Commons Attribution 4.0 International License, which permits use, sharing, adaptation, distribution and reproduction in any medium or format, as long as you give appropriate credit to the original author(s) and the source, provide a link to the Creative Commons licence, and indicate if changes were made. The images or other third party material in this article are included in the article's Creative Commons licence, unless indicated otherwise in a credit line to the material. If material is not included in the article's Creative Commons licence and your intended use is not permitted by statutory regulation or exceeds the permitted use, you will need to obtain permission directly from the copyright holder. To view a copy of this licence, visit <http://creativecommons.org/licenses/by/4.0/>.

## References

- Paul EL, Atiemo-Obeng VA, Kresta SM (2004) Handbook of Industrial Mixing - Science and Practice. Wiley, Incorporated
- Tadros TF (2016) Emulsions - formation, Stability, Industrial Applications. Walter de Gruyter GmbH & Co KG
- Abidin MIIZ, Raman AAA, Nor MIM (2013) Review on measurement techniques for drop size distribution in a stirred vessel. *Ind Eng Chem Res* 52:16085–16094
- Hu YT, Ting Y, Hu JY, Hsieh SC (2017) Techniques and methods to study functional characteristics of Emulsion systems. *J Food Drug Anal* 25:16–26. <https://doi.org/10.1016/j.jfda.2016.10.021>
- Burke I, Youssef AS, Kockmann N (2022) Design of an AI-supported Sensor for Process Relevant Parameters in Emulsification Processes. 16 Dresden Sensor-Symposium 2022 218–223. <https://doi.org/10.5162/16dss2022/P48>
- Neuendorf LM, Baygi Z, Kolloch F, Kockmann PN (2022) Implementation of a Control Strategy for Hydrodynamics of a stirred liquid–liquid extraction column based on convolutional neural networks. *ACS Eng Au* 2:369–377. <https://doi.org/10.1021/acsengineeringau.2c00014>
- Neuendorf LM, Khaydarov V, Schlander C, Kock T, Fischer J, Urbas L, Kockmann N (2023) Artificial Intelligence-based Module Type Package-compatible Smart sensors in the process industry. *Chem Ing Tech* 95:1546–1554. <https://doi.org/10.1002/cite.202300047>
- Unnikrishnan S, Donovan J, MacPherson R, Tormey D (2020) An Integrated Histogram-based vision and machine-learning classification model for Industrial Emulsion Processing. *IEEE Trans Industr Inf* 16:5948–5955. <https://doi.org/10.1109/TII.2019.2959021>
- Neuendorf L, Müller P, Lammers K, Kockmann N (2023) Convolutional Neural Network (CNN)-Based measurement of properties in Liquid–Liquid systems. *Processes* 11. <https://doi.org/10.3390/pr11051521>
- Xiouras C, Cameli F, Quilló GL, Kavousanakis ME, Vlachos DG, Stefanidis GD (2022) Applications of Artificial Intelligence and Machine Learning Algorithms to crystallization. *Chem Rev* 122:13006–13042
- Höving S, Bobers J, Kockmann N (2022) Open-source multi-purpose sensor for measurements in continuous Capillary Flow. *J Flow Chem* 12:185–196. <https://doi.org/10.1007/s41981-021-00214-w>
- Jaritsch D, Holbach A, Kockmann N (2014) Counter-current extraction in Microchannel Flow: current status and perspectives. *J Fluids Eng* 136. <https://doi.org/10.1115/1.4026608>
- Holbach A, Çalışkan E, Lee H-S, Kockmann N (2014) Process intensification in small scale extraction columns for Counter-current Operations. *Chem Eng Process* 80:21–28. <https://doi.org/10.1016/j.cep.2014.03.013>
- Reichmann F, Herath J, Mensing L, Kockmann N (2021) Gas-Liquid Mass transfer intensification for bubble generation and breakup in Micronozzles. *J Flow Chem* 11:429–444. <https://doi.org/10.1007/s41981-021-00180-3>
- Holbach A, Soboll S, Schuur B, Kockmann N (2015) Chiral separation of 3,5-Dinitrobenzoyl-(R, S)-Leucine in process intensified extraction columns. *Ind Eng Chem Res* 54:8266–8276. <https://doi.org/10.1021/acs.iecr.5b00896>
- Bobers J, Grün J, Höving S, Pyka T, Kockmann N (2020) Two-phase Flow in a coiled Flow Inverter: process development from batch to continuous Flow. *Org Process Res Dev* 24:2094–2104. <https://doi.org/10.1021/acs.oprd.0c00152>
- Au AK, Huynh W, Horowitz LF, Folch A (2016) 3D-Printed Microfluidics. *Angew Chem Int Ed* 55:3862–3881. <https://doi.org/10.1002/anie.201504382>

18. Waheed S, Cabot JM, Macdonald NP, Lewis T, Guijt RM, Paull B, Breadmore MC (2016) 3D printed microfluidic devices: enablers and barriers. *Lab Chip* 16:1993–2013
19. Maaß S, Rojahn J, Hänsch R, Kraume M (2012) Automated drop detection using image analysis for online particle size monitoring in multiphase systems. *Comput Chem Eng* 45:27–37. <https://doi.org/10.1016/j.compchemeng.2012.05.014>
20. Stieß M (2009) *Mechanische Verfahrenstechnik - Partikeltechnologie 1*. Springer Berlin Heidelberg, Berlin, Heidelberg
21. Rueger PE, Calabrese RV (2013) Dispersion of water into oil in a rotor-stator mixer. Part 1: Drop breakup in dilute systems. *Chem Eng Res Des* 91:2122–2133. <https://doi.org/10.1016/j.cherd.2013.05.018>
22. Carl Roth GmbH (2020) Sonnenblumenöl reinst. raffiniert - Sicherheitsinformationen
23. Xiao Y, Tian Z, Yu J, Zhang Y, Liu S, Du S, Lan X (2020) A review of object detection based on deep learning. *Multimed Tools Appl* 79:23729–23791. <https://doi.org/10.1007/s11042-020-08976-6>
24. Panckow RP, Reinecke L, Cuellar MC, Maa S (2017) Photo-Optical In-Situ measurement of Drop size distributions: applications in Research and Industry. *Oil Gas Sci Technol* 72. <https://doi.org/10.2516/ogst/2017009>
25. Emmerich J, Tang Q, Wang Y, Neubauer P, Junne S, Maaß S (2019) Optical Inline Analysis and monitoring of particle size and shape distributions for multiple applications: scientific and industrial relevance. *Chin J Chem Eng* 27:257–277
26. Bormashenko EY (2018) *Wetting of Real surfaces*. De Gruyter, Berlin, Boston
27. Zhao CX, Middelberg APJ (2011) Two-phase Microfluidic flows. *Chem Eng Sci* 66:1394–1411. <https://doi.org/10.1016/j.ces.2010.08.038>
28. Schneider CA, Rasband WS, Eliceiri KW (2012) NIH Image to ImageJ: 25 years of image analysis. *Nat Methods* 9:671–675. <https://doi.org/10.1038/nmeth.2089>
29. Zierp J, Bühler K (2018) *Grundzüge Der Strömungslehre*. Springer, Wiesbaden

**Publisher's Note** Springer Nature remains neutral with regard to jurisdictional claims in published maps and institutional affiliations.